Accepted by Astronomical Journal (December 2001 Issue)

CCD PHOTOMETRY OF THE CLASSIC SECOND PARAMETER GLOBULAR CLUSTERS M3 AND M13 [1]

Soo-Chang Rey[2], Suk-Jin Yoon, Young-Wook Lee
Center for Space Astrophysics & Department of Astronomy,
Yonsei University, Shinchon 134, Seoul 120-749, Korea
Electronic mail : (screy, sjyoon, ywlee)@csa.yonsei.ac.kr

Brian Chaboyer
Department of Physics and Astronomy, 6127 Wilser Lab, Dartmouth College, Hanover, NH 03755-3528
Electronic mail : chaboyer@heather.dartmouth.edu

and

Ata Sarajedini
Department of Astronomy, 211 Bryant Space Science Center, P.O. Box 112055,
University of Florida, Gainesville, FL 32611-2055
Electronic mail : ata@astro.ufl.edu

ABSTRACT

We present high-precision V, $B-V$ color-magnitude diagrams (CMDs) for the classic second parameter globular clusters M3 and M13 from wide-field deep CCD photometry. The data for the two clusters were obtained during the same photometric nights with the same instrument, allowing us to determine accurate relative ages. Based on a differential comparison of the CMDs using the $\Delta(B-V)$ method, an age difference of 1.7 ± 0.7 Gyr is obtained between these two clusters. We compare this result with our updated horizontal-branch (HB) population models, which confirm that the observed age difference can produce the difference in HB morphology between the clusters. This provides further evidence that age is the dominant second parameter that influences HB morphology.

Subject headings: color-magnitude diagrams — globular clusters: individual (M3, M13) — stars: evolution — stars: horizontal-branch

[1]Data were obtained using the 2.4 m Hiltner Telescope of the Michigan-Dartmouth-M.I.T. (MDM) Observatory.

[2]Visiting Astronomer, MDM Observatory.

1. INTRODUCTION

Since the pioneering work by Sandage & Wallerstein (1960), van den Bergh (1967), and Sandage & Wildey (1967), it has been known that, in addition to [Fe/H] (the "first parameter"), there must be a second parameter controlling the morphology of the horizontal-branch (HB) in Galactic globular clusters (GGCs). Because of its important implications for the formation chronology of the Galaxy (Searle & Zinn 1978; Lee, Demarque, & Zinn 1994, hereafter LDZ), determining the nature of this second parameter has been one of the key questions during the last forty years. The high-precision CCD photometry of GCs in recent years (Bolte 1989; Buonanno et al. 1990, 1994; Green & Norris 1990; Chaboyer, Demarque, & Sarajedini 1996; Sarajedini, Chaboyer, & Demarque 1997; Sarajedini 1997; Stetson et al. 1999; Lee & Carney 1999) and the recent advances in HB modeling (LDZ) have suggested that age is most likely the cause of the observed variations in HB morphology among clusters of the same [Fe/H] and as a function of Galactocentric distance. In particular, LDZ have concluded that age is the most natural candidate for the global second parameter, because other candidates, such as helium abundance, CNO abundance, and core rotation, can be ruled out from the observational evidence, while supporting evidence does exist for the age hypothesis.

While the above view is generally accepted, some critics have argued that the relative age differences inferred from the main-sequence turnoffs (MSTOs) are sometimes too small to explain the differences in HB morphology between second parameter clusters (VandenBerg, Bolte, & Stetson 1990, hereafter VBS; Stetson, VandenBerg, & Bolte 1996; Catelan & de Freitas Pacheco 1995; Johnson & Bolte 1998, hereafter JB98). Among them, the most problematic case is M3 and M13, which is one of the most famous second parameter pairs along with NGC 288 and NGC 362, where the age difference is well established. These studies argue that the age difference between M3 and M13 is appreciably smaller than the one suggested by HB population models, and therefore is not sufficient to explain the observed difference in HB morphologies. The difference in HB morphology between M3 and M13, however, is not as dramatic as that of NGC 362 and NGC 288, because M3, the cluster with the redder HB, possesses an intermediate HB type with both blue and red HB stars. Therefore, the predicted age difference is smaller in the M3/M13 pair (see Lee et al. 1999 and below) as compared with NGC 288/NGC 362, and is sometimes compatible with the observational uncertainties (1 - 2 Gyr) of the available CCD photometry.

Consequently, in order to test the age hypothesis of the second parameter effect between M3 and M13, high-quality CCD data should be taken that is good enough to discriminate a small age difference. For relative age dating of GGCs, it is essential to obtain CMDs that are reliable, at least, in a differential sense. The inhomogeneity of datasets and analysis methods in the various studies has been a major limitation of relative age dating of GCs. Until recently, many studies combined CMDs obtained from different instruments with different calibrations. These results have often been significantly hampered by this inhomogeneity and thus cannot be considered to be conclusive (see review in Stetson et al. 1996; Rosenberg et al. 1999). Indeed, even for the same GC, the fiducials that have been derived in different investigations sometimes show large

differences between them (e.g., see Fig. 12 of VandenBerg 2000 for M3 fiducials). Consequently, for reliable relative age dating, the CCD frames for the two clusters must be taken during the same observing run using the same instruments, and also the same reduction and calibration procedures must be employed for these frames.

Although M3 and M13, which have similar [Fe/H] values but different HB morphologies, provide a typical example of the second parameter pair, there are only a few studies based on homogeneous datasets. One of the best available CCD CMDs for M3 and M13 are provided by JB98. Their VI photometry was obtained with the same telescope during the same observing run, and the resulting CMDs for the two clusters narrowly define the cluster sequences from the red giant branch (RGB) to ~ 3 mag below the MSTO. Using the differential age dating described by VBS, they concluded that the clusters are unlikely to differ in age by the amount required to explain the differnece in their HB morphology purely as an age effect. They proposed that the observations could be explained better with a difference in the main-sequence (MS) helium abundance (with M13 having the larger helium abundance), while this contradicts the observational evidence of similar helium abundances between M3 and M13 to within the errors ($Y = 0.204^{+0.011}_{-0.012}$ vs. $0.180^{+0.023}_{-0.027}$; Sandquist 2000). On the other hand, Stetson (1998) obtained homogeneous BI photometry for M3 and M13 using the CFHT, and proposed that M13 appears to be about 12% older than M3, although he argued that age is not the only appropriate difference between M3 and M13, due to the bluer color of MSTO of M13 than that of M3 and different slopes of subgiant branches (SGBs) in these two clusters. From his preliminary instrumental $B, B-R$ CMD for M3 and M13, Sarajedini (1999) also presented a result that M13 appears to be older than M3 by ~ 2 Gyr and this age difference is consistent with that implied by HB models. Consequently, although there are at least three independent studies on the second parameter problem for M3 and M13 based on homogeneous datasets, the situation is still rather controversal.

The purpose of this paper is to present our new high-quality homogeneous BV CCD photometry of M3 and M13. Our new photometry was obtained on the same photometric nights with the same instrument producing a deeper and more extensive dataset as compared with that of JB98. This allows us to carry out a relative age dating for these clusters that is more precise than previous studies. These data are then compared with our new updated HB models to test the age hypothesis of the second parameter effect between M3 and M13.

2. OBSERVATIONS AND DATA REDUCTIONS

All the observations were made using the Michigan-Dartmouth-MIT (MDM) Observatory 2.4m telescope during two nights of an observing run in 2000 March. Images were obtained with the thinned, back-illuminated, SITE 2048 "Echelle" CCD and the standard Johnson B and V filters. The field of view of this CCD is roughly $9'.5$ with a pixel scale of $0''.28$. We observed two partially overlapping fields in M3 and M13, respectively. One field was about $12'$ south-west (SW) of the cluster center in order to produce a deep and well-defined MS in each cluster. Six long (200

- 800 s) and six short (20 - 60 s) exposures were obtained at this location. In order to ensure a large sample of SGB and RGB stars, a second field off the cluster center by $9'$ west (W) was observed with three medium (80 - 240 s) and three short (20 - 60 s) exposures. The nights were dark and of photometric quality, and the seeing was also good - in the range $1''.0$ - $1''.2$. Figure 1 and Figure 2 show the observed cluster fields for M3 and M13, respectively.

The raw data frames were calibrated using twilight and dawn sky flats and zero-level exposures. Calibration frames were made by combining several individual exposures. All exposure times were sufficiently long that the center-to-corner shutter timing error was negligible. These procedures produced object frames with the sky flat to better than 1% in all filters.

Photometry of the M3 and M13 stars was accomplished using DAOPHOT II and ALLSTAR (Stetson 1987, 1995). For each frame, a Moffat function PSF, varying quadratically with radial position, was constructed using 50 to 100 bright, isolated, and unsaturated stars. The PSF was improved iteratively by subtracting faint nearby companions of the PSF stars. We calculated aperture corrections using the program DAOGROW (Stetson 1990). Using the aperture photometry data, growth curves were constructed for each frame, in order to extrapolate from the flux measurements over a circular area of finite radius to the total flux observable for the star. The final aperture correction was made by adjusting the ALLSTAR magnitude of each star by the weighted mean of the difference between the total aperture magnitude returned by DAOGROW and the profile-fitting ALLSTAR magnitude for selected stars (e.g., PSF stars). The typical rms deviation for the aperture correction for all frames corresponds to 0.013 mag, which introduces a modest uncertainty to the zero point of the calibration equation. After the aperture correction, DAOMATCH/DAOMASTER (Stetson 1992) were then used to match stars of all frames covering the same field, and derive the average instrumental magnitude on the same photometric scale. For each frame, the magnitude offset with respect to each master frame in B and V was calculated, and photometry for all frames of the same field was transformed to a common instrumental system. In this way, robust, intensity-weighted mean instrumental magnitudes and rms scatters of magnitudes were obtained for all matched stars. Last, the mean instrumental B and V magnitudes were matched to form $B-V$ color.

On each night, a number of standard stars from the list of Landolt (1992) were observed. 63 standard stars were observed in B and V, covering a color range of –0.3 - 2.2 for $B-V$, and an airmass range of 1.16 - 1.46. All standard-star exposure times were long ($>$ 7 sec) enough so that the systematic error resulting from shutter timing ($\sim$ a few tens of milliseconds) is insignificant ($<$ 1%). DAOGROW was also performed to measure the total aperture magnitude of the standard stars. The aperture magnitudes and the known standard system magnitudes were then used to derive coefficients of the transformation equations. The atmospheric extinction coefficients in each color have been determined by the same standard stars at different airmasses. The final transformation equations were obtained by a linear least-square fit. They are

$$B - V = 1.130(b - v)_o + 0.280,$$

$$V - v_o = -0.037(B - V) - 1.118,$$

where $B - V$ and V are the color indices and visual magnitude in the standard BV system, $(b - v)_o$ and v_o refer to instrumental ones corrected for extinction. No other trends in the residuals were noticeable, and therefore no additional terms in the transformation equations appear to be necessary. The calibration equations relate observed to standard values for V and $B - V$ with rms residuals of 0.006 and 0.005 mag, respectively, as shown in Figure 3.

From comparison of the stars belonging to overlapping area of two adjacent fields, we confirmed that there are no systematic differences in either color or magnitude between the cluster fields. The mean offsets of the photometric zeropoint are never greater than 0.01 mag. We compared our CCD photometry with data taken from other studies for the stars in common. Figure 4a and Figure 5a show comparison of our V magnitudes with those of JB98 for M3 and M13 stars, respectively. The mean difference in the sense our measurements minus others is 0.002 $\pm$ 0.028 and 0.001 $\pm$ 0.024 for M3 and M13, respectively, where the uncertainty is the standard deviation of the mean. Fig. 4b shows comparisons with photometry of Stetson & Harris (1988) for M3 (their secondary standard field). The mean differences are 0.026 $\pm$ 0.019 and 0.010 $\pm$ 0.022 in V and $B - V$, respectively. We have also made a comparison with the photometry of Richer & Fahlman (1986) for M13, as shown in Fig. 5b. The mean differences are 0.019 $\pm$ 0.019 and 0.009 $\pm$ 0.014 in V and $B - V$, respectively. We conclude that there are no significant systematic zero-point differences between our photometry and others.

3. COLOR-MAGNITUDE DIAGRAMS

For the final photometric list, we selected stars with a detection on at least three frames in each band, error in the B and V magnitudes of less than 0.05 mag, and a mean value of χ (quality of the PSF fit to the stellar image returned by DAOPHOT II) less than 2. Figure 6 shows our V, $B - V$ CMDs for the M3 and M13, respectively, representing stars used in our analysis. All of the long exposure data for the SW field of M3 and M13 were included except saturated bright RGB stars which were recovered from the short exposure data. However, in the case of the W field data, the following selection criteria were adopted to have the best definitions of the CMD branches since crowding worsens the quality of the photometry in the inner cluster region. We included only stars with $V < 18$ mag from the medium exposure data of M3. For the sparsely populated bright RGB and SGB of M13, we added medium and short exposure photometry for the relatively bright stars ($V < 18.7$, $B - V > 0.3$) in outer part of the CCD frame (Y $>$ 700 pixel) to help define the sequences more accurately. In order to represent the HB blue tail of M13 which extends to about the MSTO magnitude, we include all medium exposure data with $B - V < 0.3$. Note that the CMD of M13 is being used here to understand the morphology of the CMD and does not accurately represent the population ratios of stars in different evolutionary stages. The CM data for M3 and M13 are tabulated in Table 1 and Table 2, respectively. In each table, most data are taken from the SW field, while 5000 series identifications are from the W field.

Both our M3 and M13 CMDs extend to about 3.5 magnitudes fainter than the MSTO. All of cluster sequences that we are particularly interested in (the lower RGB, SGB, MS, and MSTO) are significantly well defined, allowing us to derive the cluster parameters accurately. Our CMDs show the similar quality and overall morphology with those of previous investigators (e.g., JB98), but include more stars in all the cluster sequences. Although there is a paucity of stars in the brightest RGB and asymptotic giant branch regions in both cluster CMDs, this does not hamper our differential age analysis which mainly uses the lower RGB stars.

M13 has an exclusively blue HB with a long blue tail extending well below the level of the MSTO. Moreover, the HB appears to have two gaps at $V \sim 15.6$ and $V \sim 17.6$. These gaps are also presented in the previous BV data (Paltrinieri et al. 1998) and HST UV/visual data (Ferraro et al. 1997, 1998) at similar locations to ours. Ferraro et al. (1998) suggested that the gaps are not statistical fluctuations, but real, because gaps seem to be at similar locations (i.e., at similar T_{eff}) in different clusters (see also Piotto et al. 1999; D'Cruz et al. 2000). The two apparent gaps in our HB of M13 appear to be the G1 and G3 gaps labeled by Ferraro et al. (1998).

The fiducial line of the MS and RGB was constructed by iteratively rejecting a few stars which deviate by more than 3σ from the main branches, binning stars over 0.2 mag intervals in V, and then determining the robust mean value in V and $B-V$ for each bin. The MSTO region, which has a strong curvature and is critical for differential age dating techniques, was sampled with a smaller magnitude bin of 0.1 mag. Because of the very small number of potential members brighter than V ∼14.5 and V ∼13.5 for M3 and M13, respectively, the fiducial line of bright RGB sequence is determined by eye. Our unsmoothed M3 and M13 fiducial sequences are listed in Table 3 and Table 4, respectively. We found no significant difference between RGB fiducials from the W and SW fields. There is some disagreement of our fiducial for M13 with that of Paltrinieri et al. (1998). However, we found that our fiducial has good agreement with those obtained from other studies such as Richer & Fahlman (1988) and Yim et al. (2000). While these two fiducials agree well with ours in the region of MS and SGB, Paltrinieri et al.'s fiducial shows large deviation in this region.

4. RELATIVE AGE DATING: $\Delta(B-V)$ METHOD

In contrast to absolute age dating techniques, relative age determinations are less affected by uncertainties in stellar evolution theory, because most of the effects of theoretical uncertainties are removed in a relative comparison. Furthermore, differential comparisons between GCs can reduce the effects of observational uncertainties involved in the absolute age determination (see Stetson et al. 1996; Sarajedini et al. 1997). For example, VBS and Sarajedini & Demarque (1990) independently showed that, for clusters having similar chemical compositions, the color difference between the MSTO and the lower giant branch (and the SGB) is an excellent age diagnostic, in the sense that a larger color difference denotes a younger age; one major advantage of this diagnostic is that it is independent of distance, reddening, and photometric zero-point/color calibrations.

The technique outlined by VBS involves normalizing cluster principal sequences by the TO color, $(B-V)_{TO}$, and the visual magnitude, $V_{+0.05}$, of the MS at the point 0.05 mag redder than the TO color. Once this shifting has been accomplished, older clusters will have bluer giant branches relative to younger clusters and vice versa.

The $(B-V)_{TO}$ and $V_{+0.05}$ were determined by fitting a parabola to the stars in the region near the MSTO and upper MS point 0.05 mag redder than the TO, respectively. We derived $(B-V)_{TO} = 0.440 \pm 0.005$ and 0.435 ± 0.006 for M3 and M13, respectively, where the uncertainty is the observed scatter of the stars in the TO region. The $V_{+0.05}$ was also obtained to be 19.91 ± 0.06 and 19.49 ± 0.06 for M3 and M13, respectively, where the error is also the observed scatter of the stars within the parabola-sided boxes including $V_{+0.05}$.

In Figure 7, we show our CM data and fiducial sequences for M3 and M13 using the registration prescription specified by VBS. In Fig. 7b, also shown are Yonsei-Yale (Y^2) isochrones (Yi et al. 2001) having [Fe/H] = -1.66 [3] (Zinn & West 1984) and $[\alpha/Fe] = 0.3$ and ages ranging from 10 to 14 Gyr. The M3 and M13 sequences and the isochrones have been shifted horizontally to match at $(B-V)_{TO}$, and vertically to agree with one another at $V_{+0.05}$. As shown in the figures, the RGB sequences of M3 and M13 are well separated from each other, indicating a real age difference.

It is important to note that, in Fig. 7, the separation in the SGB region between M3 and M13 appears to be inconsistent with the original registration scheme of VBS, where the SGBs of the two clusters should be coincident. As shown in the isochrones of Fig. 7b, this separation is partly explained as a real feature if the absolute ages of the two clusters are as young as 10 - 12 Gyr. This feature was also found in the VI CMDs reported by JB98. However, their CMDs show a larger separation between the SGBs of the two clusters than ours, relative to the separation of the RGBs caused by an age difference (see Fig. 8 and Fig. 9 of JB98). VandenBerg (2000) found that this is due to the failure of JB98 to match their data in the TO region, and explained that matching the CMDs at $V_{+0.05}$ will not produce a superposition of the cluster TOs if the MS loci have different slopes.

In Fig. 7, we also see that the TO of M13 is slightly brighter than that of M3 after the cluster fiducials have been registerd following the VBS method. Following the recommended procedures of VandenBerg (2000, see his footnote 3), we therefore shifted our M13 fiducial vertically until the differences between the two clusters are minimized at the two points that are 0.05 mag redder than the TO (i.e., both above and below the TO). The M13 sequence has been shifted fainter and bluer by 0.06 mag and 0.001 mag, respectively. In Figure 8, we present our M3 and M13 fiducial sequences and individual CM data, after the TOs of both clusters are made to coincide with each other, along with the same isochrones shown in Fig. 7b. It should be noted that there is still a sufficiently large separation between the M3 and M13 RGBs, implying an age difference.

[3]Our models reveal that the Δ Age/$\Delta(B-V)$ of RGBs will not be affected by choice of [Fe/H] from -1.9 to -1.4.

The relative age is measured by comparing the colors of the RGB, where the color separation is largely independent of magnitude. In the range of -4 < $V - V_{+0.05}$ < -2, we fit a parabola to the M3 RGB sequence and calculated the mean offset between this parabola and the shifted RGB stars of M13. In order to check the reliability of this estimate, we repeated this procedures for the case of the M13 RGB sequence and the M3 stars. We find the mean value of the color difference between the RGBs, in the sense of M3 - M13, to be $\delta(B-V)_{RGB} = 0.029 \pm 0.008$. The error is the standard error of the mean color difference. We estimated $\sigma\ (B-V) = 0.008$ in the separation of the RGBs due to the error of the MSTO color. Considering the additional error (0.08 mag) from the magnitude of the MSTO which corresponds to the $\sigma\ (B-V) = 0.004$ in the RGBs, we estimated $\sigma\ (B-V) = 0.009$ due to the combined error in the magnitude and color of MSTO. When this error is combined with that of the mean color difference between the RGBs, the total uncertainty of the color difference between the RGBs of M3 and M13 corresponds to 0.012 mag.

We calculate the offset in RGB color associated with an offset in presumed age by noting that $\Delta(logt_9)$ = -2.19$\Delta(B-V)$. This corresponds to about 0.59 Gyr per 0.01 mag, if we adopt an age of 12 Gyr for M13. It should be noted that the color difference between the RGBs is not uniform, but depends on the absolute age (see the spacing of isochrones presented in Fig. 7 and 8), in the sense that using younger isochrones would reduce the inferred age differences. Adopting the absolute age of M13 to be about 12 Gyr (Chaboyer et al. 1998; Yi et al. 2001), the color difference between the two clusters corresponds to a relative age difference of 1.7 ± 0.7 Gyr, in the sense that M13 is older. [4, 5]

[4]Note that a difference in [O/Fe] is unlikely to account for the difference in $\Delta(B-V)$ between M3 and M13. This is because M13 would need to have a higher [O/Fe] value ($\sim$ 0.8 dex at [Fe/H] = -1.6 and 12 Gyr, see VandenBerg & Stetson 1991) than M3 and if this is the case, then the HB of M13 would be redder than that of M3 (LDZ). This situation is the opposite of what is observed in these two clusters. On the other hand, from a measurement of the oxygen abundance in relatively less evolved stars near the base of the RGB (i.e., in the vicinity of the first dredgeup), Pilachowski & Armandroff (1996) suggested that M13 is as much as Δ[O/Fe] $\sim$ 0.3 dex more oxygen poor than M3, while this is still a disputable result (see Kraft et al. 1997). If true, this oxygen abundance difference will increase the inferred age difference ($\sim$ 0.7 Gyr, see VandenBerg & Stetson 1991), since the effects of decreasing [O/Fe] are to increase the $\Delta(B-V)$ of M13 at a given age.

[5]In order to check the dependence of derived age difference on the part of the RGB which is considered, we derived age difference between M3 and M13 in the range of -3 < $V - V_{0.05}$ < -2 and -4 < $V - V_{0.05}$ < -3, separately. We find the mean value of the color difference between RGBs, in the sense of M3 - M13, to be $\delta(B-V)_{RGB} = 0.027 \pm 0.008$ and 0.030 ± 0.008, respectively. From the isochrones, we also calculate $\Delta(logt_9)$ = -2.39$\Delta(B-V)$ and $\Delta(logt_9)$ = -2.08$\Delta(B-V)$, respectively. This corresponds to about 0.64 Gyr and 0.56 Gyr per 0.01 mag. Therefore, the color differences between the two clusters correspond to the relative age differences of 1.73 Gyr and 1.68 Gyr, respectively, which show good agreement with our adopted relative age difference (1.7 Gyr).

5. COMPARISON WITH SYNTHETIC HORIZONTAL-BRANCH MODELS

There are several recent developments that affect the relative age dating from HB morphology. We have included them in our most updated version of the HB population models (see Lee et al. 1999; Lee & Yoon 2001, in preparation). First of all, there is now reason to believe that the absolute ages of the oldest GGCs is reduced to about 12 Gyr, as suggested by the Hipparcos distance calibration and other improvements in stellar models (Reid 1998; Gratton et al. 1997; Chaboyer et al. 1998; Grundahl, VandenBerg, & Andersen 1998; Yi et al. 2001). This has a strong impact on the relative age estimation from HB morphology, because the variation of the HB mass is more sensitive to age at younger ages, due to the nonlinear relationship between RGB tip mass (M_{RG}) and age (see LDZ). Second, in the new population models, we have used new HB tracks with improved input physics (Yi et al. 1997) and corresponding Y^2 isochrones (Yi et al. 2001). Third, it is now well established that the α-elements are enhanced in halo populations. Specifically, we adopted [α/Fe] = 0.3 for clusters with [Fe/H] $<$ -1.0, and thereafter we assume that it steadily declines to 0.0 at solar metallicity (e.g., Wheeler, Sneden, & Truran 1989). In practice, the treatment suggested by Salaris, Chieffi, & Straniero (1993) was used to simulate the effect of α-element enhancement. Finally, empirical mass-loss law of Reimers (1975) suggests more mass-loss at larger ages. The result of this effect was also presented in LDZ, but unfortunately their most widely used diagram (their Fig. 7) is the one based on fixed mass-loss.

We found that all of the above effects make the HB morphology more sensitive to age. Figure 9 illustrates the HB morphology vs. [Fe/H] relations for the GGCs, along with the theoretical HB isochrones that were produced by our synthetic HB models. As shown in Fig. 9b, now the required age difference is significantly reduced as compared to LDZ. Only 1.1 Gyr of age difference, rather than 2 Gyr, is enough to explain the systematic shift of the HB morphology between the inner and outer halo clusters. To within the observational uncertainties, age differences of about 1 - 2 Gyr are now enough to explain the observed differences in HB morphology between M3 and M13 (or M2), and between the outer halo clusters (Pal 3, Pal 4, Pal 14, and Eridanus) and M3. These values are consistent with the observations presented in this paper and also with the recent relative age datings both from HST and high-quality ground-based data (Stetson et al. 1999; Lee & Carney 1999).

In Figure 10, the observed CMDs of M3 and M13 are compared with our new population models, which include the scatter expected from the random errors in magnitude and in color as estimated by our photometry. For the two clusters, we adopted the same metallicity ([Fe/H] = -1.66) on the Zinn & West (1984) scale, mass dispersion (σ_M = 0.025 $M_\odot$) on the HB, MS helium abundance (Y_{MS} = 0.23), and α-element enhancement ([α/Fe] = 0.3), but applied an age difference of 1.7 Gyr between the two clusters as estimated from our relative age dating (see Sec. 4). As shown in the figure, there is a reasonable match between the synthetic HB models and the observations. However, the observations indicate that M13 has a long blue tail on the HB, while the standard HB model (with $\sigma_M \sim$ 0.02 - 0.03 $M_\odot$) fails to reproduce this detail.

The wide color range of the M13 HB would be reproduced by using a larger value for σ_M, roughly twice as large as M3, together with a slightly larger age difference (Δt $\sim$ 2.4 Gyr) between the two clusters (see Lee & Yoon 2001, in preparation). Certainly, this uncertainty has some impact on the age difference that one infers from HB morphology. However, the magnitude of this age uncertainty ($\sim$ 0.7 Gyr) is still compatible with the errors ($\sim$ 0.7 Gyr) of the relative age dating from MSTO photometry and/or additional age difference ($\sim$ 0.7 Gyr) due to the possible difference of [O/Fe] between two clusters (see footnote 4). This suggests that the difference in age between M3 and M13 inferred from their MSTOs can account for most of the difference in the HB distribution between the two clusters. Hence, age appears to be predominantly responsible for the second parameter effect in the M3/M13 pair despite the current uncertainty about the origin of M13's blue HB extension (see Sec. 6 for discussion).

6. DISCUSSION

Although the presence of a blue tail on the HB has only a mild impact on the relative age dating from HB morphology, it is still important to understand the origin of this effect in order to use the HB as a more reliable age indicator. The blue tail phenomenon is widely considered to be a result of local effects, such as enhanced mass-loss in high density environments. Buonanno et al. (1997) examined the role of stellar density in the morphology of the HB, and suggested that clusters with higher central densities are more likely to populate the bluest extremes of the HB (see also Fusi Pecci et al. 1993). However, the correlation between stellar density and HB morphology is rather weak with large scatter and/or limited to a small fraction of GCs within an intermediate metallicity range (LDZ; Sarajedini et al. 1997). Note that the central densities (log ρ = 3.51 vs. 3.33, Harris 1996) and concentration (c = log r_t/r_c = 1.84 vs. 1.51, Harris 1996) parameters for M3 and M13 are very similar despite their apparent difference in σ_M on the HB. Furthermore, as suggested by LDZ, there is also no clear evidence that the variation of HB morphology with galactocentric distance is related to central densities of GCs.

It is also suggested that some noncanonical effects in the stellar interior, such as rapid rotation and deep mixing would make a star both bluer and brighter on the HB, and are thus related to the presence of blue tails (Mengel & Gross 1976; Kraft et al. 1993, 1997; Kraft 1994; Peterson, Rood, & Crocker 1995; Langer & Hoffmann 1995; Sweigart 1997a, 1997b; Cavallo & Nagar 2000). However, the predicted increase in the rotation velocity with effective temperature along the HB has not been confirmed from the recent high-resolution spectroscopy of blue HB stars of M13 (Behr et al. 2000). On the other hand, Behr et al. (1999) reported that, in the hotter HB stars of M13, helium is underabundant, while iron and other metals are enhanced. It is suggested that these abundance anomalies are most likely due to the diffusion effects in the radiative atmospheres. Similarly, a number of interesting phenomena have recently been reported to occur in blue HB stars around a temperature of 11,000 K; these include a gap (i.e., G1 gap) in the HB distribution (Ferraro et al. 1998; Piotto et al. 1999; Caloi 1999), a jump in the Strömgren u magnitudes and

the onset of radiative levitation (Grundahl et al. 1998, 1999), and a shift to lower surface gravities (Moehler et al. 1999, 2000). All of these phenomena suggest the blue tail feature may be related to the disappearance of surface convection and the formation of a radiative stellar atmosphere followed by radiative levitation of heavy elements and helium diffusion for stars hotter than about 11,000 K (Sweigart 2001; Moehler et al. 1999). On the theoretical point of view, it is probably possible that the levitation of heavy elements along with helium diffusion would push the blue HB stars to even hotter T_{eff} on the HR diagram, creating the blue tail. If this is confirmed by detailed modeling, the blue tail phenomenon may not be considered as adding noise to the second parameter effect, since it is then rather a general feature of extremely blue HB clusters. In this case, a more reasonable relative age would be estimated from the HB morphology by ignoring the blue tail, since radiative levitation and diffusion effects are not included in our standard HB models (i.e., Fig. 10).

7. SUMMARY

We present new high-quality V, $B-V$ CMDs for the Galactic globular clusters M3 and M13 constructed from wide-field deep CCD photometry obtained during the same nights with the same instrument. From our homogeneous dataset, we draw the following conclusions:
1. Based on a careful differential comparison of the CMDs using the $\Delta(B-V)$ method, we confirm a significant difference between these two clusters, indicating an age difference of 1.7 ± 0.7 Gyr in the sense that M13 is older than M3.
2. We present updated HB models, which suggest that HB morphology is more sensitive to cluster age compared to our previous models. From a comparison of observations with the new HB models, we find that the observed age difference can reproduce the difference in HB morphology between the clusters. This provides further evidence that cluster age is the dominant second parameter that influences HB morphology, which in turn suggests that HB morphology is a reliable age indicator in most population II stellar systems.
3. While the physical origin of the blue tail phenomenon is still uncertain, there is now a growing body of evidence that suggest this is an ubiquitous characteristic of clusters with extremely blue HB stars hotter than 11,000 K. If true, the presence of blue tail would have less impact on relative age dating based on HB morphology.

We would like to thank J. Johnson for providing electronic copy of data and an anonymous referee for a careful review and useful comments. Support for this work was provided by the Creative Research Initiative Program of Korean Ministry of Science & Technology. B. C.'s research is supported in part by NASA grant NAG5-9225. A. S. acknowledges financial support from a National Science Foundation CAREER grant No. AST-0094048.

REFERENCES

Behr, B. B., Cohen, J. G., McCarthy, J. M., & Djorgovski, S. G. 1999, ApJ, 517, L135

Behr, B. B., Djorgovski, S. G., Cohen, J. G., McCarthy, J. M., Côté, P., Piotto, G., & Zoccali, M. 2000, ApJ, 528, 849

Bolte, M. 1989, AJ, 97, 1688

Buonanno, R., Buscema, G., Fusi Pecci, F., Richer, H. B., & Fahlman, G. G. 1990, AJ, 100, 1811

Buonanno, R., Corsi, C., Fusi Pecci, F., Fahlman, G. G., & Richer, H. B. 1994, ApJ, 430, L121

Buonanno, R., Corsi, C., Bellazzini, M., Ferraro, F. R., & Fusi Pecci, F. 1997, AJ, 113, 706

Caloi, V. 1999, A&A, 343, 904

Catelan, M., & de Freitas Pacheco, J. A. 1995, A&A, 297, 345

Cavallo, R. M., & Nagar, N. M. 2000, AJ, 120, 1364

Chaboyer, B., Demarque, P., & Sarajedini, A. 1996, ApJ, 459, 558

Chaboyer, B., Demarque, P., Kernan, P. J., & Krauss, L. M. 1998, ApJ, 494, 96

D'Cruz, N. L., O'Connell, R. W., Rood, R. T., et al. 2000, AJ, 530, 352

Ferraro, F. R., Paltrinieri, B., Fusi Pecci, F., Cacciari, C., Dorman, B., & Rood, R. T. 1997, ApJ, 484, L145

Ferraro, F. R., Paltrinieri, B., Fusi Pecci, F., Rood, R. T., & Dorman, B. 1998, ApJ, 500, 311

Fusi Pecci, F., Ferraro, F. R., Bellazzini, M., Djorgovski, S., Piotto, G., & Buonanno, R. 1993, AJ, 105, 1145

Gratton, R. G., Fusi Pecci, F., Carretta, E., Clementini, G., Corsi, C. E. & Lattanzi, M. 1997, ApJ, 491, 749

Green, E. M., & Norris, J. E. 1990, ApJ, 353, L17

Grundahl, F., VandenBerg, D. A., & Andersen, M. I. 1998, ApJ, 500, L179

Grundahl, F., Catelan, M., Landsman, W. B., Stetson, P. B., & Andersen, M. I. 1999, ApJ, 524, 242

Harris, W. E. 1996, AJ, 112, 1487

Johnson, J. A., & Bolte, M. 1998, AJ, 115, 693 (JB98)

Kraft, R. P. 1994, PASP, 106, 553

Kraft, R. P., Sneden, C., Langer, G. E., & Shetrone, M. D. 1993, AJ, 106, 1490

Kraft, R. P., Sneden, C., Smith, G. H., Shetrone, M. D., Langer, G. E., & Pilachowski, C. A. 1997, AJ, 113, 279

Landolt, A. V. 1992, AJ, 104, 340

Langer, G. E., & Hoffman, R. D. 1995, PASP, 107, 1177

Lee, J.-W., & Carney, B. W. 1999, AJ, 118, 1373

Lee, Y.-W., Yoon, S.-J., Lee, H.-c., & Woo, J.-H. 1999, in ASP Conf. Ser. 192, Spectrophotometric Dating of Stars and Galaxies, ed. I. Hubeny, S. R. Heap, & R. H. Cornett (San Francisco: ASP), 185

Lee, Y.-W., Demarque, P., & Zinn, R. 1994, ApJ, 423, 248 (LDZ)

Mengel, J. G., & Gross, P. G. 1976, Ap&SS, 41, 407

Moehler, S., Sweigart, A. V., Landsman, W. B., Heber, U., & Catelan, M. 1999, A&A, 346, L1

Moehler, S., Sweigart, A. V., Landsman, W. B., & Heber, U. 2000, A&A, 360, 120

Paltrinieri, B., Ferraro, F. R., Fusi Pecci, F., & Carretta, E. 1998, MNRAS, 293, 434

Peterson, R. C., Rood, R. T., & Crocker, D. A. 1995, ApJ, 453, 214

Pilachowski, C. A., & Armandroff, T. E. 1996, AJ, 111, 1175

Piotto, G., Zoccali, M., King, I. R., Djorgovski, S. G., Sosin, C., Rich, R. M., & Meylan, G. 1999, AJ, 118, 1727

Reid, I. N. 1998, AJ, 115, 204

Reimers, D. 1975, Mem. Soc. Roy. Sci. Leige, 6th Ser., 8, 369

Richer, H. B., & Fahlman, G. G. 1986, ApJ, 304, 273

Rosenberg, A., Saviane, I., Piotto, G., & Aparicio, A. 1999, AJ, 118, 2306

Salaris, M., Chieffi, A., & Straniero, O. 1993, ApJ, 414, 580

Sandage, A., & Wallerstein, G. 1960, ApJ, 131, 598

Sandage, A., & Wildey, R. 1967, ApJ, 150, 469

Sandquist, E. L. 2000, MNRAS, 313, 571

Sarajedini, A. 1997, AJ, 113, 682

Sarajedini, A. 1999, in ASP Conf. Ser. 165, The Third Stromlo Symposium: The Galactic Halo, ed. B. K. Gibson, T. S. Axelrod, & M. E. Putman (San Francisco: ASP), 295

Sarajedini, A., & Demarque, P. 1990, ApJ, 365, 219

Sarajedini, A., Chaboyer, B., & Demarque, P. 1997, PASP, 109, 1321

Searle, L., & Zinn, R. 1978, ApJ, 225, 357

Stetson, P. B. 1987, PASP, 99, 191

Stetson, P. B. 1990, PASP, 102, 932

Stetson, P. B. 1992, in IAU Colloq. 136, Stellar Photometry-Current Techniques and Future Developments, ed. C. J. Butler & I. Elliot (Cambridge: Cambridge University Press), 291

Stetson, P. B. 1995, DAOPHOT II User's Manual (Victoria: Dominian Astrophys. Obs.)

Stetson, P. B. 1998, CFHT Information Bulletin No. 38

Stetson, P. B., VandenBerg, D. A., & Bolte, M. 1996, PASP, 108, 560

Stetson, P. B., Bolte, M., Harris, W. E., et al. 1999, AJ, 117, 247

Stetson, P. B., & Harris, W. E. 1988, AJ, 96, 909

Sweigart, A. V. 1997a, ApJ, 474, L23

Sweigart, A. V. 1997b, in The Third Conference on Faint Blue Stars, ed. A. G. D. Philip, J. Liebert, & R. A. Saffer (Cambridge: Cambridge University Press), 3

Sweigart, A. V. 2001, to appear in Highlights of Astronomy, Vol 12 (astro-ph/0103133)

VandenBerg, D. A. 2000, ApJS, 129, 315

VandenBerg, D. A., & Stetson, P. B. 1991, AJ, 102, 1043

VandenBerg, D. A., Bolte, M., & Stetson, P. B. 1990, AJ, 100, 445 (VBS)

van den Bergh, S. 1967, AJ, 72, 70

Wheeler, J. C., Sneden, C., & Truran, J. W. 1989, ARAA, 27, 279

Yi, S., Demarque, P., & Kim, Y.-C. 1997, ApJ, 482, 677

Yi, S., Demarque, P., Kim, Y.-C., Lee, Y.-W., Ree, C. H., Lejeune, T., & Barnes, S. 2001, ApJS, in press

Yim, H.-S., Byun, Y.-I., Sohn, Y.-J., & Chun, M.-S. 2000, AJ, 120, 872

Zinn, R., & West, M. J. 1984, ApJS, 55, 45

Table 1. CCD Photometry for M3*

ID	x	y	V	σ_V	$B-V$	$\sigma_{(B-V)}$
1	1467.63	1106.58	11.406	0.005	0.702	0.007
2	644.02	26.79	12.853	0.004	1.426	0.006
3	241.15	354.39	14.047	0.003	0.664	0.005
4	285.23	1191.12	14.165	0.003	1.024	0.005
5	1559.35	1816.76	14.840	0.003	0.804	0.005
6	400.20	1052.79	15.180	0.003	1.119	0.005
7	286.05	484.68	15.349	0.003	0.851	0.005
8	313.97	470.24	15.392	0.006	0.389	0.008
9	99.29	227.80	15.415	0.005	0.550	0.007
10	835.15	1745.64	15.540	0.006	0.820	0.008
..	.....	.....	.....	.....	.....	.....
..	.....	.....	.....	.....	.....	.....
..	.....	.....	.....	.....	.....	.....
5001	640.73	649.51	12.741	0.023	1.415	0.024
5002	1505.17	209.86	13.510	0.006	1.188	0.009
5003	1847.97	271.11	14.019	0.008	1.057	0.010
5004	1155.44	72.02	14.265	0.006	0.909	0.009
5005	930.84	1552.24	14.538	0.006	0.978	0.008
..	.....	.....	.....	.....	.....	.....
..	.....	.....	.....	.....	.....	.....
..	.....	.....	.....	.....	.....	.....

*Table 1 is presented in its complete form in the electronic edition of the Astronomical Journal. The first page of this table is presented here for guidance regarding its form and content.

Table 2. CCD Photometry for M13*

ID	x	y	V	σ_V	$B-V$	$\sigma_{(B-V)}$
1	466.76	880.00	14.242	0.005	0.573	0.007
2	322.68	1512.17	14.308	0.004	0.889	0.006
3	144.05	115.67	14.503	0.004	0.844	0.006
4	1373.81	235.60	14.721	0.004	0.597	0.006
5	54.15	183.29	14.736	0.004	0.824	0.006
6	453.66	688.43	14.889	0.004	0.581	0.006
7	1697.89	520.95	15.030	0.004	1.379	0.006
8	400.83	97.12	15.045	0.004	0.788	0.006
9	893.09	604.51	15.063	0.004	0.073	0.006
10	98.33	687.16	15.076	0.004	0.076	0.006
..	.....	.....	.....	.....	.....	.....
..	.....	.....	.....	.....	.....	.....
..	.....	.....	.....	.....	.....	.....
5001	530.49	325.30	11.973	0.007	1.552	0.009
5002	1571.01	281.42	12.203	0.006	1.306	0.009
5003	1024.98	160.02	12.488	0.007	1.297	0.009
5004	647.51	16.39	12.668	0.008	1.182	0.010
5005	1518.46	258.04	12.708	0.008	1.200	0.010
..	.....	.....	.....	.....	.....	.....
..	.....	.....	.....	.....	.....	.....
..	.....	.....	.....	.....	.....	.....

*Table 2 is presented in its complete form in the electronic edition of the Astronomical Journal. The first page of this table is presented here for guidance regarding its form and content.

Table 3. M3 fiducial sequence

V	$B-V$	V	$B-V$
14.72	0.928	19.50	0.456
15.24	0.863	19.71	0.474
15.83	0.806	19.89	0.489
16.31	0.759	20.10	0.507
16.80	0.727	20.30	0.538
17.09	0.712	20.51	0.562
17.25	0.699	20.70	0.595
17.53	0.688	20.91	0.627
17.69	0.669	21.10	0.668
17.89	0.669	21.30	0.709
18.11	0.644	21.50	0.749
18.31	0.614	21.70	0.798
18.49	0.520	21.91	0.846
18.69	0.457	22.09	0.873
18.91	0.445	22.29	0.895
19.10	0.438	22.48	0.941
19.30	0.447	.....	.....

Table 4. M13 fiducial sequence

V	$B-V$	V	$B-V$
13.75	0.943	18.68	0.436
14.25	0.876	18.90	0.444
14.76	0.821	19.10	0.457
15.25	0.775	19.31	0.469
15.76	0.734	19.51	0.485
16.24	0.701	19.69	0.508
16.77	0.668	19.90	0.531
17.13	0.654	20.10	0.564
17.29	0.639	20.31	0.603
17.49	0.631	20.50	0.637
17.70	0.613	20.69	0.678
17.90	0.532	20.90	0.712
18.11	0.464	21.10	0.763
18.29	0.443	21.30	0.800
18.51	0.436	21.49	0.837

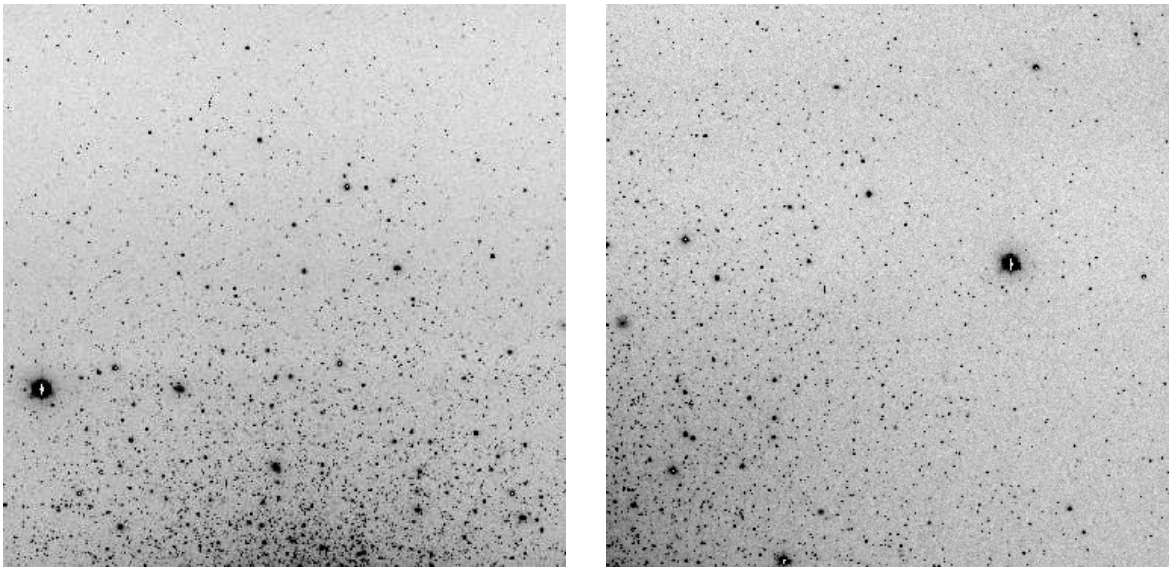

Fig. 1.— Observed cluster regions in (a) west and (b) south-west field of M3. North is to the left and east is down.

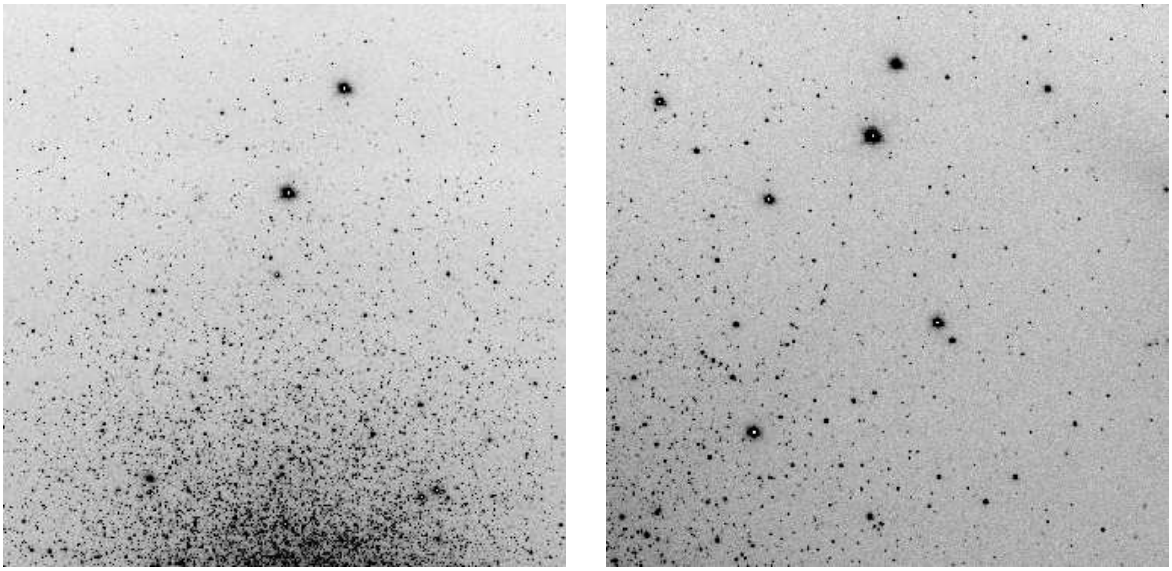

Fig. 2.— Observed cluster regions in (a) west and (b) south-west field of M13. North is to the left and east is down.

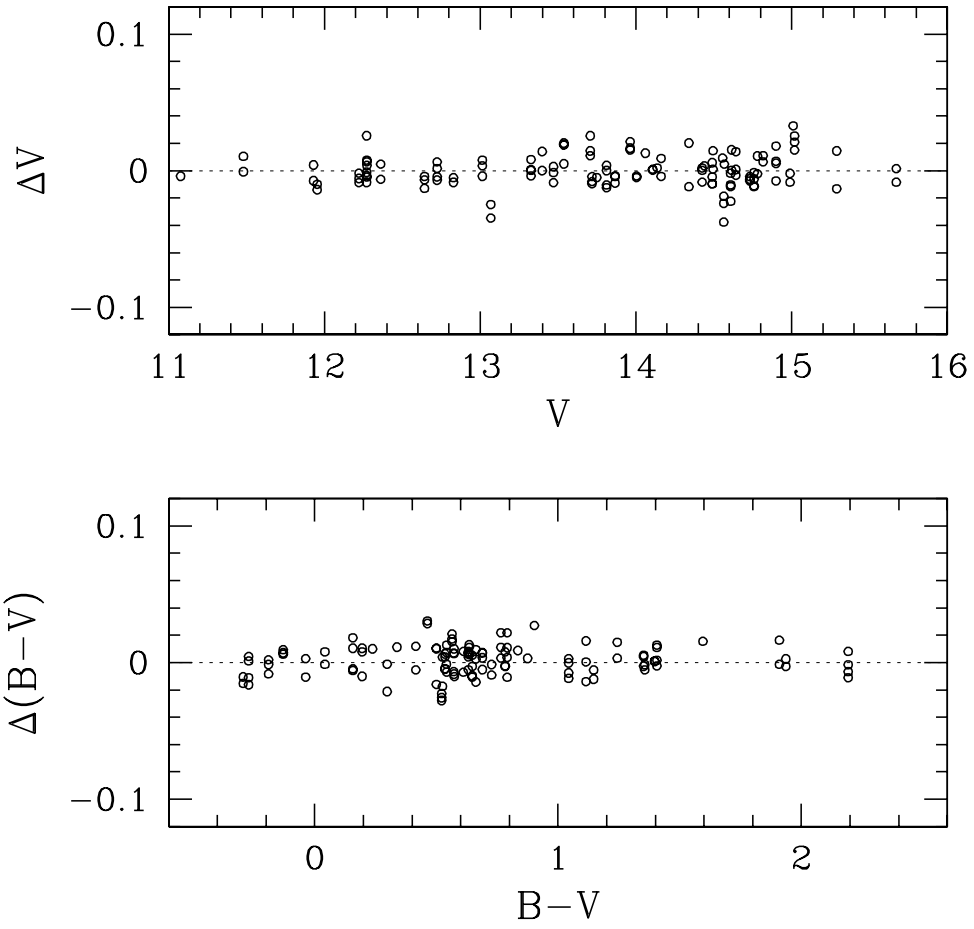

Fig. 3.— Magnitude and color residuals for the comparison of Landolt (1992) standards and measured values in this study, in the sense of us minus Landolt.

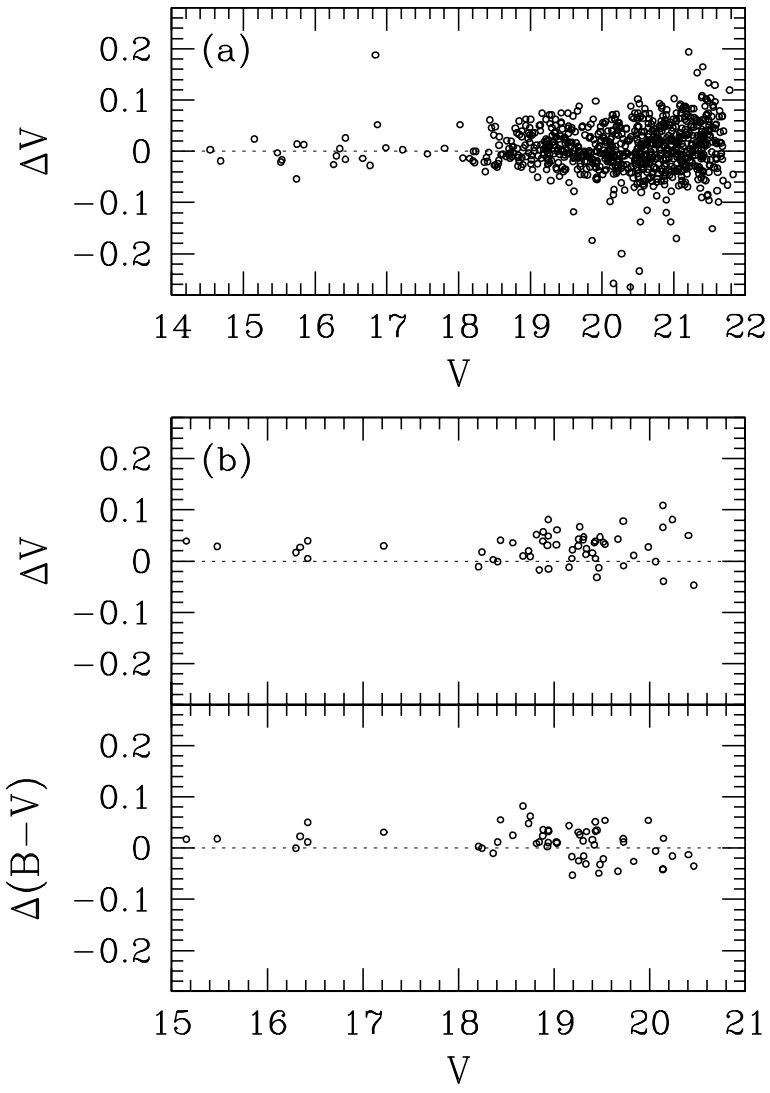

Fig. 4.— Comparison of our photometry with (a) Johnson & Bolte (1998) and (b) Stetson & Harris (1988) for M3. The differences are in the sense of our photometry minus others.

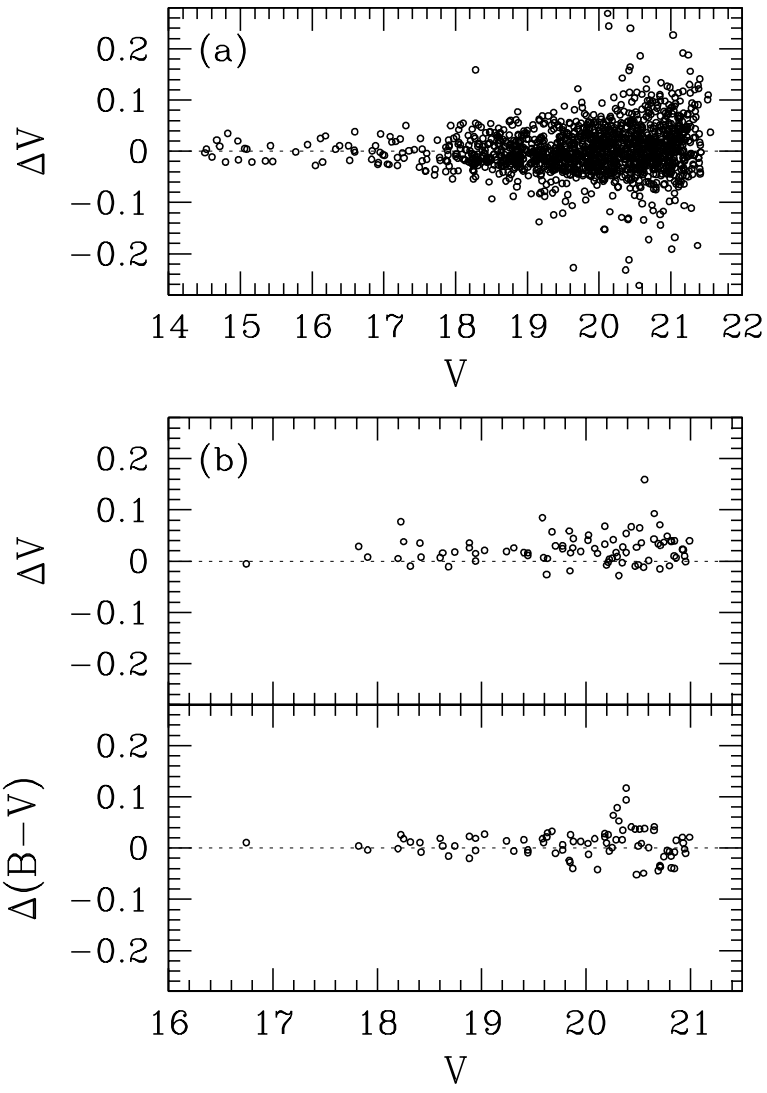

Fig. 5.— Comparison of our photometry with (a) Johnson & Bolte (1998) and (b) Richer & Fahlman (1986) for M13. The differences are in the sense of our photometry minus others.

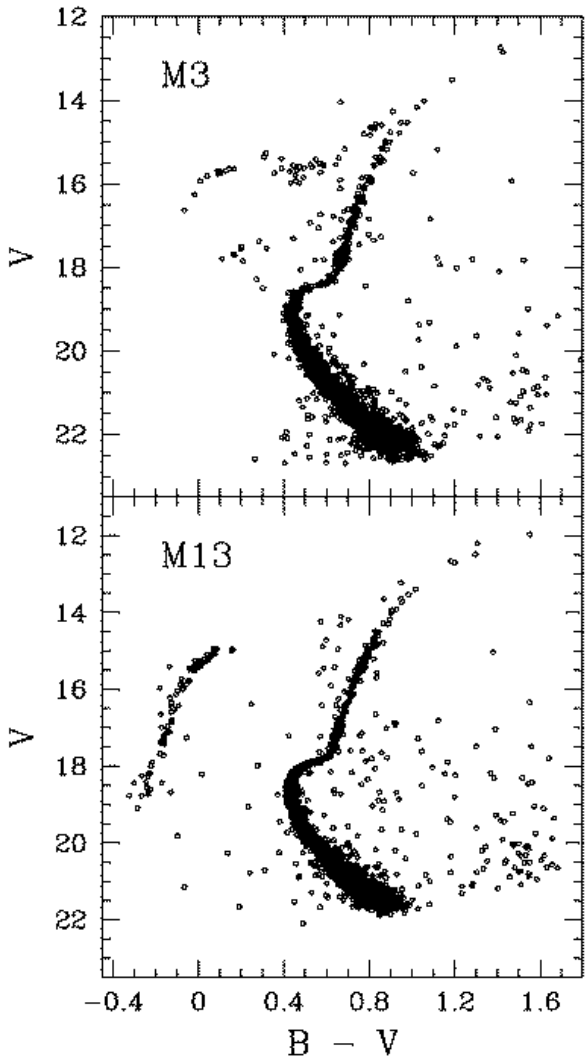

Fig. 6.— $(V, B-V)$ CMDs for M3 (top) and M13 (bottom). See the text for the adopted selection criteria that provide the best definitions of the CMD sequences.

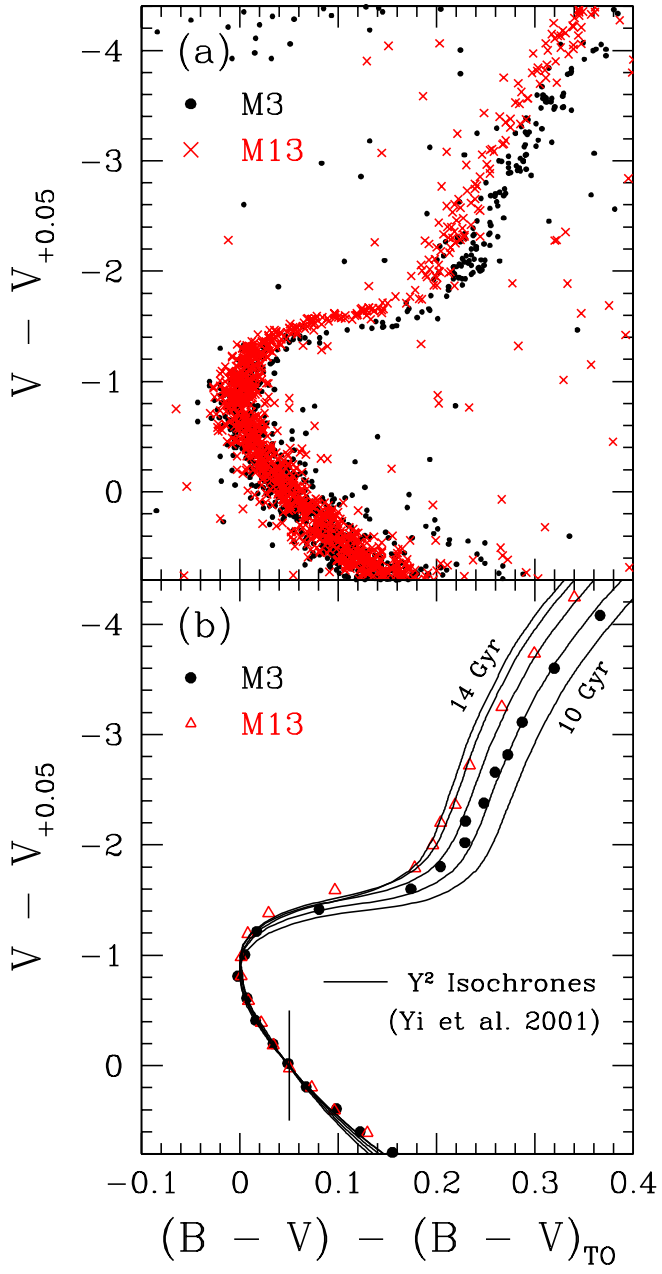

Fig. 7.— (a) Comparison of our CM data of M3 (black filled circles) and M13 (red crosses), using the registration prescription specified by VBS. (b) Same as (a) but for the fiducial sequences. We also included Yonsei-Yale (Y^2) Isochrones (Yi et al. 2001) having [Fe/H] = -1.66 and [α/Fe] = 0.3 and ages ranging from 10 to 14 Gyr. Note the large separation between the M3 and M13 RGBs, and slight offset in the SGB region.

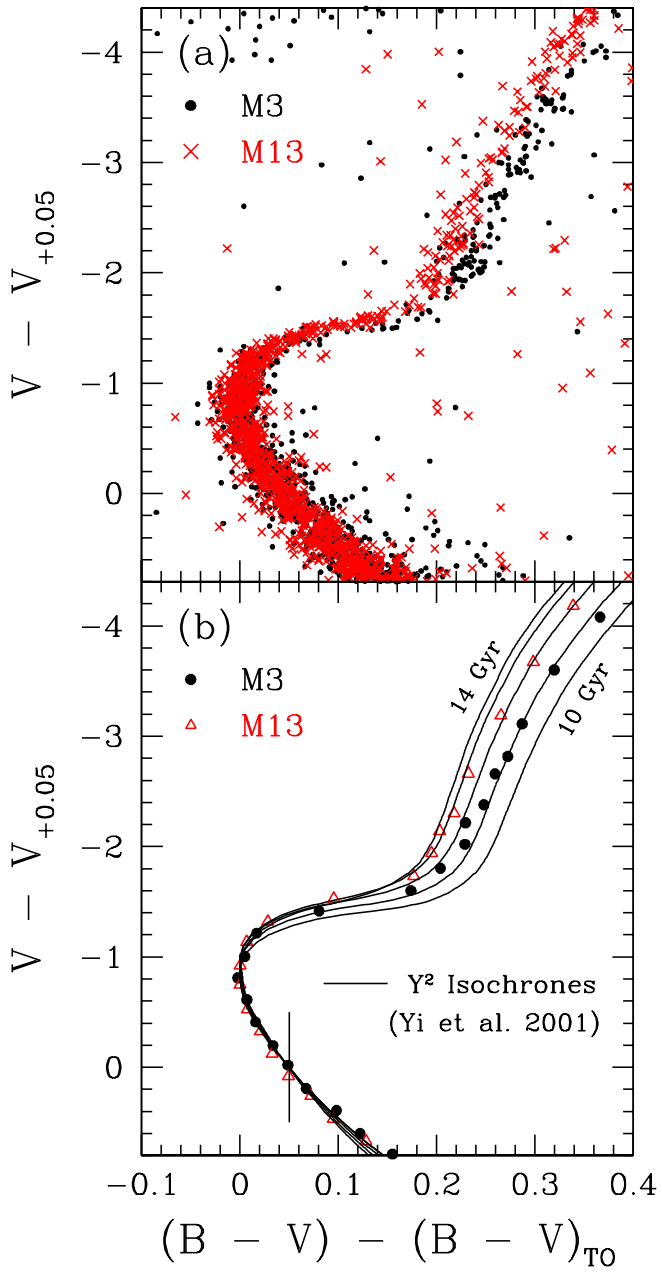

Fig. 8.— Same as Fig. 7, but after the M13 sequence has been shifted in order to make the TOs of both clusters coincide with each other (see text). Note that there is still a sufficiently large separation between the M3 and M13 RGBs, implying a true age difference.

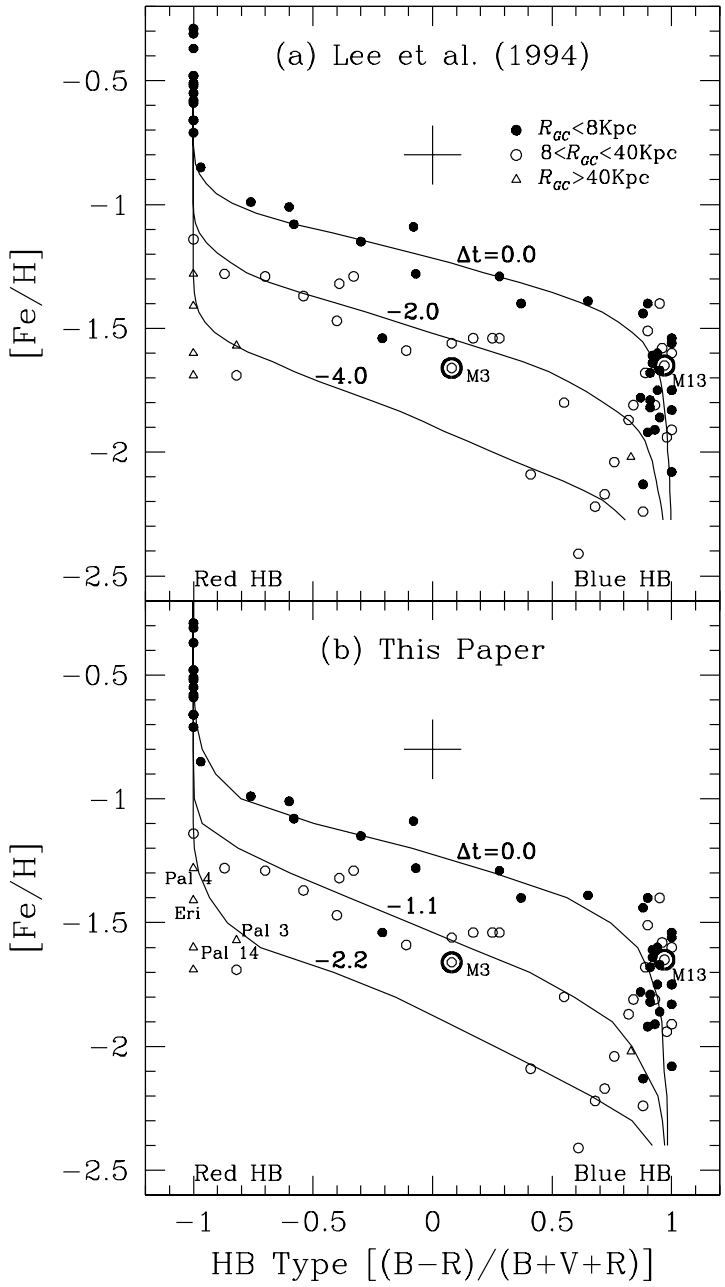

Fig. 9.— HB morphology vs. [Fe/H] relations for Galactic globular clusters with theoretical isochrones that were produced by synthetic HB models (cluster data from Table 1 of LDZ). Our new HB models with the effects of recent developments (b) are more sensitive to age compared to our earlier models (a). $\Delta t = 0$ corresponds to the mean age of the inner halo (R < 8 kpc) clusters, and the relative ages are in Gyr. Note that, with our new HB models, age differences of about 1 - 2 Gyr are now enough to explain the observed differences in HB morphology between M3 and M13.

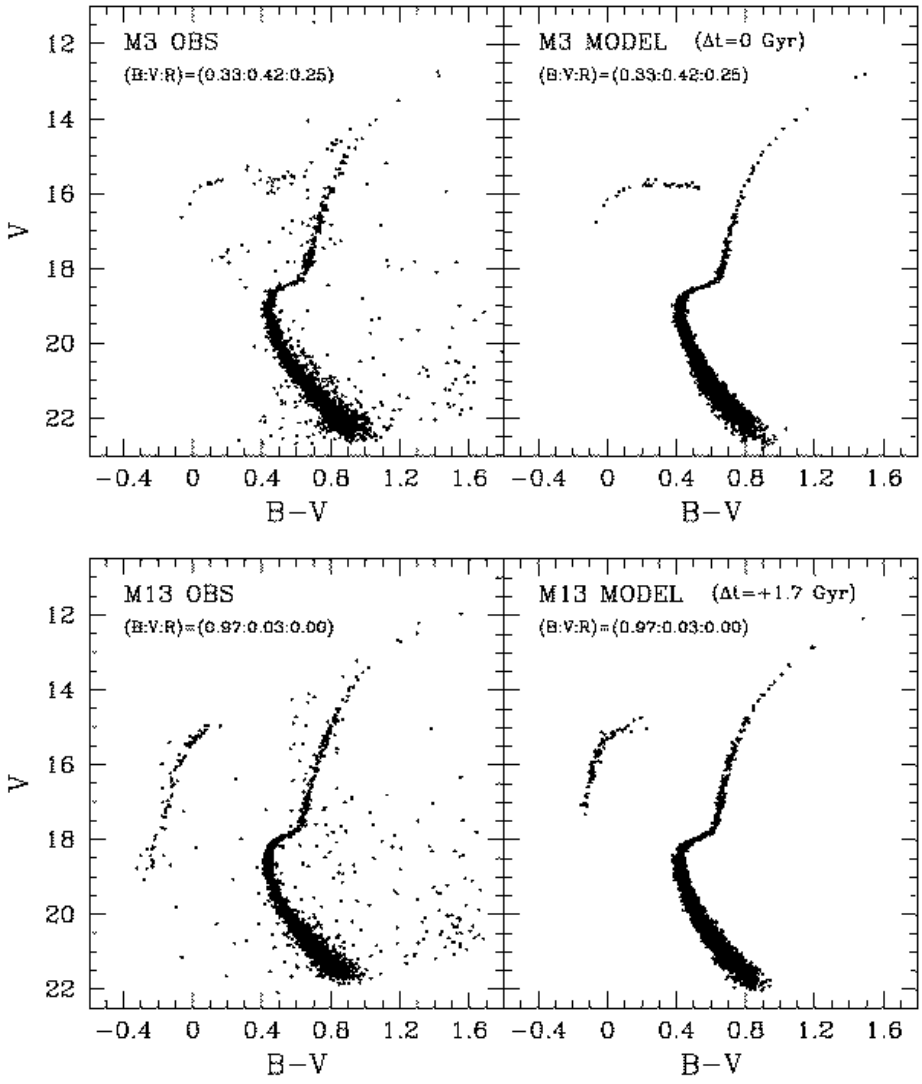

Fig. 10.— Comparison of observational and synthetic CMDs for M3 and M13, assuming that M13 is older by 1.7 Gyr. Crosses in the model CMDs are RR Lyrae variables.